



HAL
open science

Volumetric properties of carbon dioxide + acrylic acid binary in the context of supercritical precipitation polymerization

Matías Menossi, Juan Milanesio, Séverine Camy, Simon Harrisson, Miriam Strumia, Mathias Destarac

► **To cite this version:**

Matías Menossi, Juan Milanesio, Séverine Camy, Simon Harrisson, Miriam Strumia, et al.. Volumetric properties of carbon dioxide + acrylic acid binary in the context of supercritical precipitation polymerization. *Journal of Supercritical Fluids*, 2020, 160, pp.104787. 10.1016/j.supflu.2020.104787 . hal-02614169

HAL Id: hal-02614169

<https://hal.science/hal-02614169v1>

Submitted on 2 Jun 2020

HAL is a multi-disciplinary open access archive for the deposit and dissemination of scientific research documents, whether they are published or not. The documents may come from teaching and research institutions in France or abroad, or from public or private research centers.

L'archive ouverte pluridisciplinaire **HAL**, est destinée au dépôt et à la diffusion de documents scientifiques de niveau recherche, publiés ou non, émanant des établissements d'enseignement et de recherche français ou étrangers, des laboratoires publics ou privés.



Open Archive Toulouse Archive Ouverte




OATAO is an open access repository that collects the work of Toulouse researchers and makes it freely available over the web where possible

This is an author's version published in: <http://oatao.univ-toulouse.fr/25859>

Official URL:

<https://doi.org/10.1016/j.supflu.2020.104787>

To cite this version:

Menossi, Matías and Milanesio, Juan M. and Camy, Séverine  and Harrisson, Simon  and Strumia, Miriam and Destarac, Mathias  *Volumetric properties of carbon dioxide + acrylic acid binary in the context of supercritical precipitation polymerization.* (2020) *The Journal of Supercritical Fluids*, 160. 104787. ISSN 0896-8446.

Any correspondence concerning this service should be sent to the repository administrator: tech-oatao@listes-diff.inp-toulouse.fr

Volumetric properties of carbon dioxide + acrylic acid binary in the context of supercritical precipitation polymerization

Matías Menossi^a, Juan M. Milanesio^{a,*}, Séverine Camy^b, Simon Harrisson^c,
Miriam Strumia^a, Mathias Destarac^d

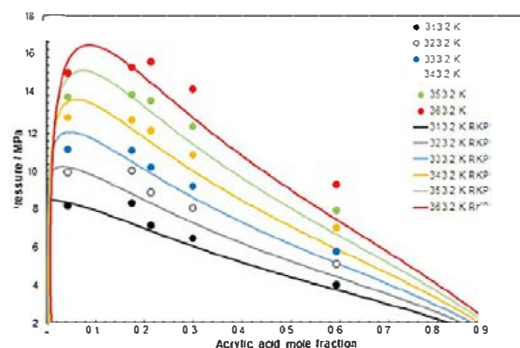
^a Instituto de Investigación y Desarrollo en Ingeniería de Procesos y Química Aplicada (IPQA-UNC-CONICET), Av. Vélez Sarsfield 1611, Ciudad Universitaria, X5016GCA, Córdoba, Argentina

^b Laboratoire de Génie Chimique, Université de Toulouse, CNRS, INPT, UPS, Toulouse, France

^c Laboratoire de Chimie des Polymères Organiques (LCPO), CNRS, ENSCBP University of Bordeaux, UMR 5629, 16, av. Pey Berland, 33607 Pessac Cedex, France

^d Laboratoire des IMRCP, Université de Toulouse, CNRS UMR 5623, Université Paul Sabatier, 118 route de Narbonne, 31062, Toulouse Cedex 9, France

GRAPHICAL ABSTRACT



ABSTRACT

Keywords:

Carbon dioxide
Acrylic acid
Density
Liquid-vapor equilibrium
High-pressure

Acrylic acid can be polymerized by precipitation in different solvents. Carbon dioxide is an interesting solvent given its tunable density and solvent power depending on the pressure and temperature. These physicochemical characteristics make it possible to solubilize some polar compounds in CO₂ depending on temperature and pressure. In this work, we report pressure vs volume pseudo-continuous curves at constant temperature for the CO₂ + AA binary mixture. They were determined in a fully computerized variable-volume high-pressure view cell capable of monitoring the position of the piston. The experimental data is simultaneously isoplethic and isothermal and it covers a wide range of pressures (up to 20 MPa). Using this raw experimental data, other properties were determined such as liquid-vapor phase boundaries, density and excess volumes. The temperature range was 313.15–363.15 K and the mole fraction of AA in the mixture was increased from 0.044 to 0.594.

1. Introduction

Carbon dioxide (CO₂) capture, utilization and storage, including conversion to valuable chemicals, are contemporary issues with several challenges [1]. The replacement of conventional organic solvents by more benign compounds has a considerable interest

* Corresponding author.

E-mail address: juan.milanesio@unc.edu.ar (J.M. Milanesio).

in new technologies with the aim of reducing waste streams [2]. CO₂ has many unique properties and constitutes an increasingly popular alternative in polymer processing [2]. Is a low dielectric constant compound and a weak Lewis acid with a significant quadrupole moment. Further, CO₂ is a gas at normal conditions but, compressed, can reach the supercritical domain ($T_C = 304.25$ K, $P_C = 7.38$ MPa) at relatively moderate conditions. CO₂ has interesting properties in the supercritical region including tunable density and solvent power, intermediate viscosities between vapor and liquid viscosities and “liquid-like” heat capacity depending on pressure and temperature [3]. Particularly, in polymer synthesis, CO₂ has other interesting advantages, such as high mass transport rates, no Trommsdorff effect and no chain transfer to solvent [2]. Supercritical CO₂ can solubilize low molecular weight polar molecules such as ethanol, acetone, tetrahydrofuran [4], and even some carboxylic acids such as acrylic acid (AA) [5]. Therefore, supercritical CO₂ (scCO₂) can also be used as a reaction medium in radical polymer synthesis, as many unsaturated monomers are soluble at relatively moderate conditions [6–8]. However, the corresponding polymers are typically insoluble in scCO₂, giving rise to a typical heterogeneous polymerization.

Hydrophilic polymers can be obtained by various heterogeneous polymerization processes in organic solvent, including precipitation, inverse emulsion, suspension and dispersion polymerizations. These systems differ in the initial phase behavior of the polymerization mixture, polymerization kinetics, and mechanism of particle formation [9]. Although widely used, these processes sometimes require purification steps. Desorption of the surfactant from particles and removal of volatile organic compounds (VOCs), like residual monomer and/or solvent from the polymer, are among the drawbacks of these processes [10]. Precipitation polymerization is a stabilizer-free process in which both initiator and monomer are soluble in the reaction medium while the polymer is insoluble and precipitates as it is formed and allows the preparation of high-purity polymer powders [11].

Poly(acrylic acid) (PAA) is used in many applications: as a superabsorbent polymer for hygiene products and agriculture, scale inhibitor for water treatment and dispersant for paints and the paper industry. On an industrial scale, it is produced either by solution free-radical polymerization in water or in heterogeneous media [12]. AA has been polymerized successfully in CO₂ by precipitation polymerization in a batch reactor [2,11,13,14] and by continuous precipitation polymerization in Continuous Stirred Tank Reactors (CSTR) [7]. To properly design supercritical reactors, it is important to consider the phase behavior of the initial reactive mixture. In this context, one of the main goals of the present work is to experimentally find conditions of homogeneity for the binary mixture CO₂ + AA at different temperatures to carry out the initial stages of the polymerization in single fluid phase conditions. On the other hand, density data is important for the design of continuous supercritical reactors, given that the volumetric flow rates and the residence time are related to this property of the fluid mixture. To experimentally find conditions of homogeneity for the solvent mixtures, an isothermal/isoplethic method was used in this work, with a continuous scan of the pressure and the density of the mixture. This method was developed by Prof. Kiran's group and there are several publications showing its importance [15–17].

The main goal of this work is to provide new experimental data on phase boundaries at different temperature and volumetric data for the 'CO₂ + AA' binary system. Pressure vs Volume pseudo-continuous curves at constant temperature were determined in a variable volume high-pressure view cell, in a wide range of pressures. As part of these experiments, liquid-vapor boundaries were determined, and Density vs Pressure and Density vs Temperature plots were built. Six different mixture compositions were loaded to the cell from 0.044 to 0.594 mol fraction of AA in

the 313.15–363.15 K temperature range. The maximum pressure recorded was 20 MPa and the maximum density 980 kg/m³. With this volumetric data, excess volume plots at high pressure for the mixture were obtained, resulting in negative deviations. The experimental window swept in this work is in accordance with the polymerization conditions described previously in the literature for AA in CO₂ [7,11,13,14]. The phase boundaries were correlated with a simple model. A three-parameter cubic equation of state (3P-EoS), the RKPR EoS, developed by Cismondi et al. [18], was applied in order to improve the representation of densities for different types of compounds, while maintaining the relative simplicity of cubic equations of state. This EoS has shown to predict very well the phase behavior of CO₂-containing mixtures [19–21], but this is the first time, to our knowledge, that is applied to a carboxylic acid binary system. This work forms part of a wider project involving the copolymerization of AA and other comonomers in compressed solvents.

2. Materials and methods

2.1. Materials

SEPPIC (Toulouse, France) provided acrylic acid (AA) (79-10-7 CAS number) 97% pure, according to gas chromatography (GC) containing 200 ppm of inhibitor (monomethylether of hydroquinone (MEHQ)) and it was used without further purification. Carbon dioxide (CO₂) (124-38-9 CAS number) with a purity of 99.95 % (GC) was purchased from Air Liquide (Toulouse, France) and was used as received.

2.2. Experimental setup and operational procedures

The volumetric data and phase boundaries were obtained in a variable volume high pressure cell (Top Industrie N° 2607 0000) that incorporates a linear variable differential transducer (LVDT) for continuous sensing of the position of the movable piston inside the variable-volume part of the cell. A motorized screw is connected to the back part of the piston and is used to change the inner volume of the system and, therefore, the pressure. The volume, pressure and temperature of the system together with the rate of increasing or decreasing volume can be controlled and recorded by the software provided with the phase equilibrium cell. Temperature was measured by a thermocouple (J type, precision of ± 0.1 K) placed in the center of the cell. Pressure was measured using a pressure transducer (Keller, precision of ± 0.13 MPa) equipped with a pressure numerical display. The body of the view cell is built in stainless steel and it has internal tubing for temperature control. The maximum internal volume of the cell is 31.8×10^{-5} m³ while the minimum volume is 9.8×10^{-5} m³. These values were confirmed by measuring the mass of a low surface tension solvent, i.e. n-hexane, that can be loaded into the cell at the maximum (minimum piston stroke) and minimum volume (maximum piston stroke). A sapphire window permits visual observations as well as the recording of the system (by using the camera (5), see Fig. 1) during a given experiment. The temperature of the cell is controlled using a circulation bath (Lauda Eco Silver) and tubing incorporated in the body of the cell as it was described above. Fig. 1 shows a diagram of the phase equilibrium cell used in this work.

In a typical experiment, liquid AA is charged to the cell using a regular syringe through the inlet port (10) (see Fig. 1) The mass of AA is weighted in a Sartorius analytical balance with a weighing range of 1×10^{-5} –0.2 kg and a weighing uncertainty of 1×10^{-7} kg. The amount of acid transferred is measured gravimetrically. Carbon dioxide is charged through the inlet valve (6), connected to a high pressure electronically controlled syringe pump (Top Industrie PMHP 100–500). The amount of carbon dioxide charged is deter-

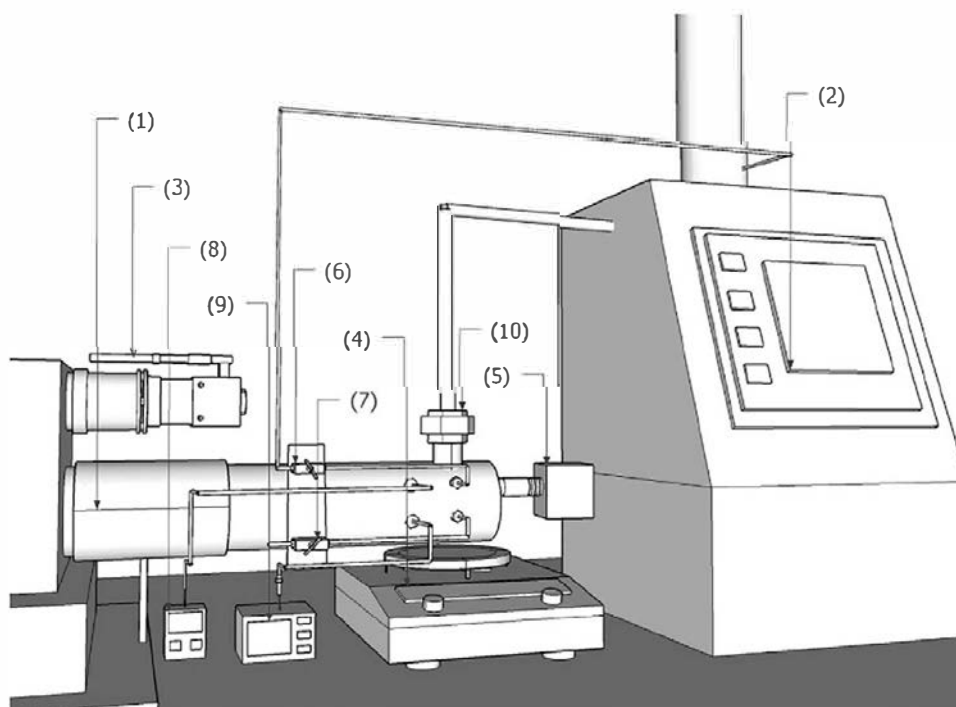


Fig. 1. Schematic diagram of the experimental setup: (1): High-pressure view cell, (2): Syringe pump, (3): Motorized piston driver, (4): Magnetic stirrer, (5): Camera, (6): Inlet valve, (7): Purge valve, (8): Pressure transducer, (9): Temperature sensor, (10): Inlet port for liquids.

mined from the initial and final conditions in the head of the syringe pump. Initially, the temperature and the pressure of the head are set at T^* and P^* . At those conditions, the CO_2 must be in the liquid state. The volume V^* occupied by the carbon dioxide in the head of the syringe is registered. Then, the inlet valve (6) of the cell is opened, letting the carbon dioxide flow into the cell. The pressure in the head of the syringe pump decreases. Finally, the inlet valve (6) is closed and the pressure and the temperature of the syringe are stabilized again at T^* and P^* . The new volume V^{**} occupied by the carbon dioxide in the head of the syringe ($V^{**} < V^*$) is registered.

The density of carbon dioxide at T^* and P^* is computed from CO_2 p-V-T information from the NISTweb book database [22]. The mass of carbon dioxide loaded into the cell is obtained simply by multiplication of the density of CO_2 obtained from NIST by the difference in volume ($V^* - V^{**}$). Total charge was typically about 0.014 kg. After charging the system, the cell is heated to the temperature and the piston is set at the maximum volume of the system, while mixing the content with a magnetic stirring bar (4) (see Fig. 1). Once mechanical and thermal equilibrium is observed (no change in pressure or temperature of the system), the piston is slowly moved forward until the maximum pressure (20 MPa) or the minimum volume of the cell ($9.8 \times 10^{-5} \text{ m}^3$) is reached. Pressure, temperature and volume of the cell are recorded during the piston stroke. Once the maximum pressure or the minimum volume is reached, the screw moves the piston backward to its initial position. Under a continuous and slow pressure change, the fluid experiences a smooth expansion or compression. During these changes in volume, the thermal circulation bath compensates for any thermal changes associated with expansion or compression of the fluid. The experiments can be considered to be under quasi equilibrium state conditions. The rate of volume change was $2.5 \times 10^{-8} \text{ m}^3/\text{s}$ for each isotherm. Fig. 2 shows typical pressure vs time raw data obtained in an experiment. This particular data set corresponds to about 800 data points with data being recorded every 2s during the scans. There is a good reproducibility of the piston position and pressure along the forward and backward direction (i.e. there is no hysteresis effect) of the scans at the rate of volume change ($2.5 \times 10^{-8} \text{ m}^3/\text{s}$).

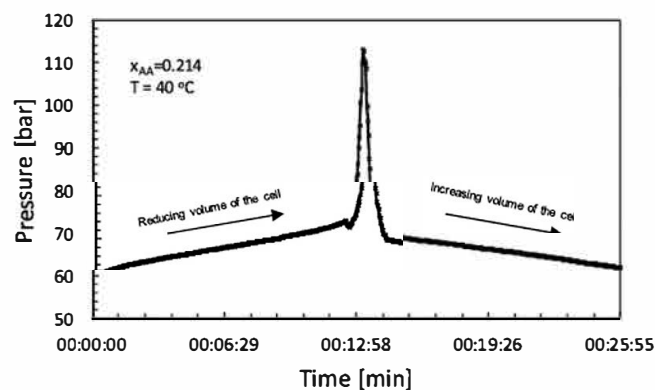


Fig. 2. Typical pressure vs time raw data obtained in the high-pressure phase equilibrium cell. Acrylic acid mole fraction of the mixture is 0.214 and the temperature 343.15 K.

The differences in pressure were 0.5 MPa maximum and they can be attributed to the piston seal friction against the inner cylinder walls of the cell. It is important to note that the pressure transducer is in the back of the piston. This methodology was previously described elsewhere [15–17] but for the first time was applied to this experimental setup.

The primary sources of error in the determination of density are linked to the uncertainties on the exact amount of the fluid CO_2 charged into the cell, and the errors associated with the LVDT reading and its relation to the position of the piston. Measurements were conducted using pure CO_2 and compared with NIST database. The average error in density was estimated to be less than 5%. A propagation of the error analysis is provided in the Supplementary Material, studying the effect of the error in the pressure, temperature and CO_2 and AA masses loaded to the cell in the informed AA mole fraction.

The sudden change in the pressure vs time slope corresponds to the change in the phase scenario inside the cell. The isothermal compressibility of the liquid mixture is much lower than the two-

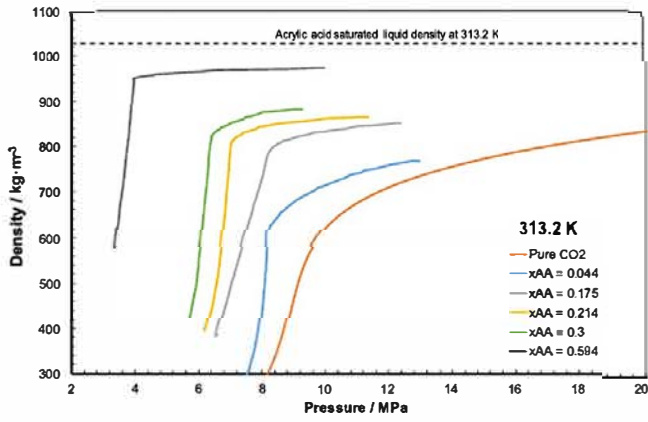


Fig. 3. Density vs pressure at constant overall composition (x_{AA}) and constant temperature (313.2 K) for the system AA + CO₂.

Experimental data:

- (—) $x_{AA} = 0.0$ (data from NIST [22]);
- (—) $x_{AA} = 0.044$ (this work);
- (—) $x_{AA} = 0.175$ (this work);
- (—) $x_{AA} = 0.214$ (this work);
- (—) $x_{AA} = 0.300$ (this work);
- (—) $x_{AA} = 0.594$ (this work);
- (—) AA saturated liquid density at 313.2 K [23].

x_{AA} : AA mole fraction.

phase liquid-vapor mixture. Therefore, the lower slope segments in Fig. 3 correspond to compression or decompression of a single liquid-like phase, and the steeper slope segments correspond to compression or decompression of a liquid-vapor two-phase mixture. The break point (pressure, temperature, composition and density of the mixture) is considered to be the bubble point of the mixture.

2.3. Modeling

Equations of state (EoS) are the proper type of models to correlate and predict the fluid phase behavior of mixtures over a wide range of conditions. Experimental data for the AA + CO₂ binary system were correlated using the RKPR-EoS [18]. The expression for RKPR-EoS explicit in pressure, is as follows:

$$P = \frac{RT}{v-b} - \frac{a}{(v+\delta_{1,EoS}b) \left(v + \frac{1-\delta_{1,EoS}}{1+\delta_{1,EoS}}b \right)} \quad (1)$$

Where, P is the absolute pressure, T is the absolute temperature, v is the molar volume, a and b are the attractive energy parameter and the repulsive co-volume parameter respectively, and R is the universal gas constant. The RKPR-EoS introduces a third parameter $\delta_{1,EoS}$, which allows to improve the reproduction of PvT data for pure compounds. In a mixture, $\delta_{1,EoS}$ depends on a linear mixing rule. For more details about RKPR-EoS see Ref. [18]. In thiswork, the attractive parameter a and the repulsive parameter b in the binary mixture are obtained using quadratic mixing rules with classic van der Waals combining rules with both an attractive and a repulsive interaction parameter k_{12} and l_{12} .

3. Results and discussion

3.1. Density

The densities for CO₂ + AA binary system have been determined for five different solutions containing increasing amounts of AA: 0.044, 0.175, 0.214, 0.300 and 0.594 mol fraction of AA. The tem-

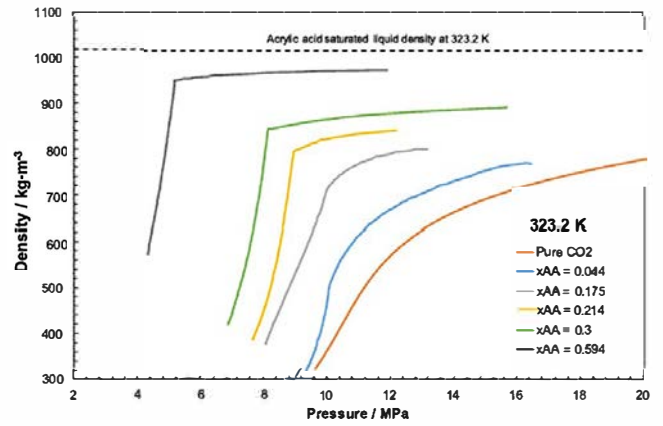


Fig. 4. Density vs pressure at constant overall composition (x_{AA}) and constant temperature (323.2 K) for the system AA + CO₂.

Experimental data:

- (—) $x_{AA} = 0.0$ (data from NIST [22]);
- (—) $x_{AA} = 0.044$ (this work);
- (—) $x_{AA} = 0.175$ (this work);
- (—) $x_{AA} = 0.214$ (this work);
- (—) $x_{AA} = 0.300$ (this work);
- (—) $x_{AA} = 0.594$ (this work);
- (—) AA saturated liquid density at 323.2 K [23].

x_{AA} : AA mole fraction.

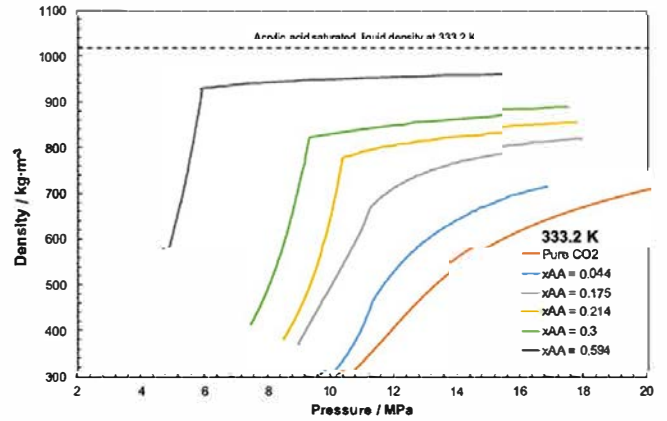


Fig. 5. Density vs pressure at constant overall composition (x_{AA}) and constant temperature (333.2 K) for the system AA + CO₂.

Experimental data:

- (—) $x_{AA} = 0.0$ (data from NIST [22]);
- (—) $x_{AA} = 0.044$ (this work);
- (—) $x_{AA} = 0.175$ (this work);
- (—) $x_{AA} = 0.214$ (this work);
- (—) $x_{AA} = 0.300$ (this work);
- (—) $x_{AA} = 0.594$ (this work);
- (—) AA saturated liquid density at 333.2 K [23].

x_{AA} : AA mole fraction.

peratures where the experiments were carried out were: 313.15, 323.15, 333.15, 343.15, 353.15 and 363.15 K and the pressure up to 20 MPa. In all determinations, the scan rates were $2.5 \times 10^{-8} \text{ m}^3/\text{s}$, to avoid possible errors in pressure caused by the friction of the piston seals. Figs. 3–8 show the density isotherms for each of the mixtures. The pure CO₂ isotherms were extracted from NIST database [22]. Also, in dashed lines, the density for saturated pure AA at the corresponding temperature is shown. They were introduced in the plots for illustration purposes and represent the limits in density for both pure compounds. The data shows the expected

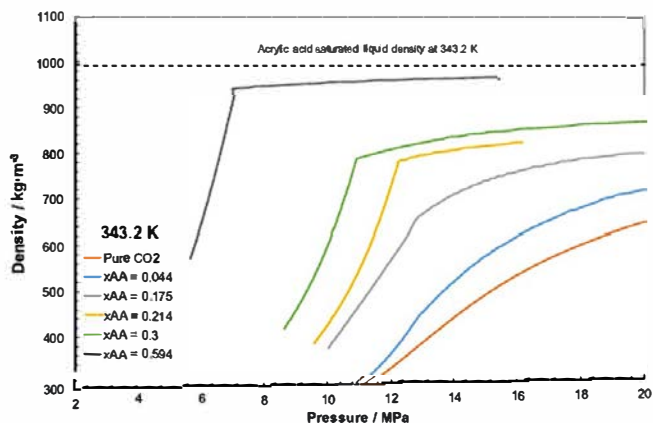


Fig. 6. Density vs pressure at constant overall composition (x_{AA}) and constant temperature (343.2 K) for the system AA + CO₂. Experimental data:

- (—) $x_{AA} = 0.0$ (data from NIST [22]);
 - (—) $x_{AA} = 0.044$ (this work);
 - (—) $x_{AA} = 0.175$ (this work);
 - (—) $x_{AA} = 0.214$ (this work);
 - (—) $x_{AA} = 0.300$ (this work);
 - (—) $x_{AA} = 0.594$ (this work);
 - (—) AA saturated liquid density at 343.2 K [23].
- x_{AA} : AA mole fraction.

trends: the density, at a given temperature, increases in going from pure CO₂ to AA richer mixtures and they become less compressible when the AA mole fraction is increased. This means that, for a given change in pressure, the relative change in density is less in AA-rich mixtures than in CO₂-rich mixtures. Also, in the single-phase region (i.e. at pressures above the break point), for a given composition, increasing pressure results in increasing densities. Figs. 9–14 show the variation of density with temperature at selected pressures for each mixture in the homogeneous liquid regions. As the raw experimental density data was acquired as a function of pres-

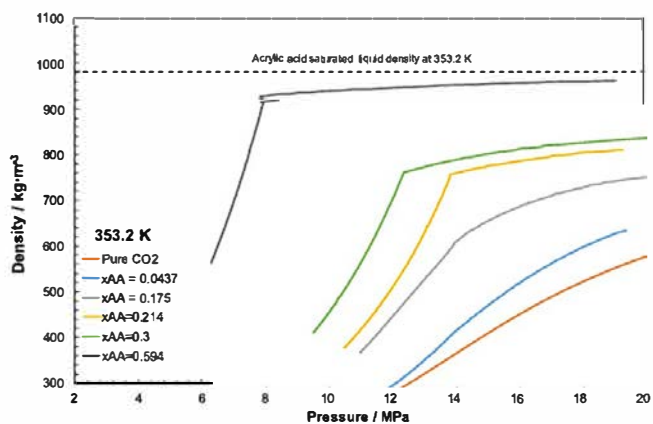


Fig. 7. Density vs pressure at constant overall composition (x_{AA}) and constant temperature (353.2 K) for the system AA + CO₂. Experimental data:

- (—) $x_{AA} = 0.0$ (data from NIST [22]);
 - (—) $x_{AA} = 0.044$ (this work);
 - (—) $x_{AA} = 0.175$ (this work);
 - (—) $x_{AA} = 0.214$ (this work);
 - (—) $x_{AA} = 0.300$ (this work);
 - (—) $x_{AA} = 0.594$ (this work);
 - (—) AA saturated liquid density at 353.2 K [23].
- x_{AA} : AA mole fraction.

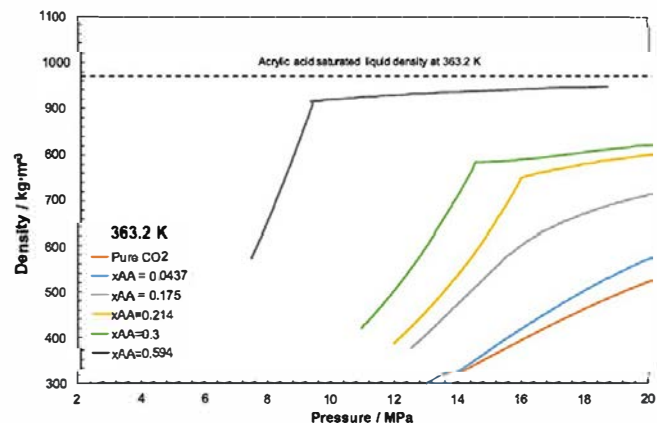


Fig. 8. Density vs pressure at constant overall composition (x_{AA}) and constant temperature (363.2 K) for the system AA + CO₂. Experimental data:

- (—) $x_{AA} = 0.0$ (data from NIST [22]);
 - (—) $x_{AA} = 0.044$ (this work);
 - (—) $x_{AA} = 0.175$ (this work);
 - (—) $x_{AA} = 0.214$ (this work);
 - (—) $x_{AA} = 0.300$ (this work);
 - (—) $x_{AA} = 0.594$ (this work);
 - (—) AA saturated liquid density at 363.2 K [23].
- x_{AA} : AA mole fraction.

sure at constant composition from the phase equilibrium cell, the density data as a function of temperature (different isobars at constant composition) was obtained by intercepting the isopleths of Figs. 3–8 at a constant pressure and registering the density values for different temperatures. This explains the fewer experimental data points in Figs. 9–14 compared with Figs. 3–8. The continuous lines were added to facilitate the visualization of the trends. As expected, at a given composition, the density of the mixture increases with increasing pressure. For a given isobar, increasing temperature decreases the mixture density, and this effect is less pronounced for AA-rich mixtures. For example, for the mixture with $x_{AA} = 0.594$ (Fig. 14), at a pressure of 13 MPa, the variation in the density between 333.15 and 363.15 K is around 30 kg/m³, while

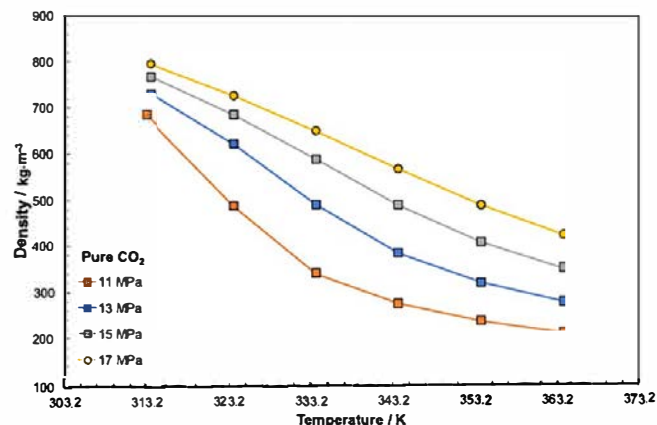


Fig. 9. Density vs temperature at constant pressure for pure CO₂. Experimental data from NIST [22]:

- (—) P = 11 MPa;
 - (—) P = 13 MPa;
 - (—) P = 15 MPa;
 - (—) P = 17 MPa;
- The straight lines were added to facilitate visualization.

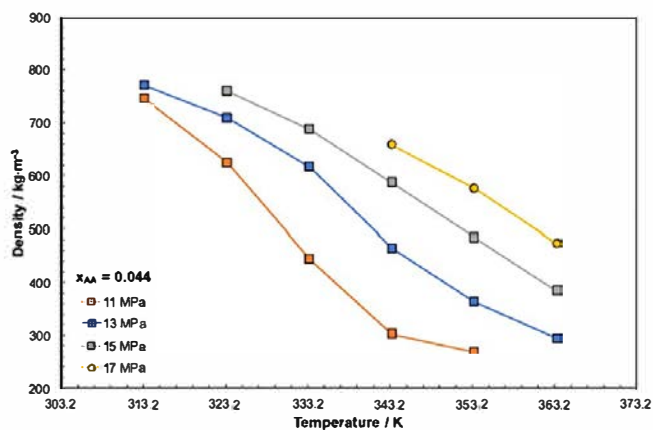


Fig. 10. Density vs temperature at constant overall composition ($x_{AA} = 0.044$) and constant pressure for the system AA + CO₂.

Experimental data (this work):

- (—■—) P = 11 MPa;
- (—■—) P = 13 MPa;
- (—■—) P = 15 MPa;
- (—●—) P = 17 MPa;

x_{AA} : AA mole fraction.

The straight lines were added to facilitate visualization.

for the mixture with $x_{AA} = 0.175$ (Fig. 11) at the same pressure and temperature range, the variation in density is more than 300 kg/m³. To our knowledge, there are no previous publications that report densities for CO₂ + AA at high pressures. Therefore, no direct comparison can be made with existing data. Nevertheless, in the next section, phase boundaries determined in this work were compared with literature data. The sudden slope changes in the isotherms indicate the phase boundaries. This break point is much clearer with increasing AA content in the mixture.

Figs. 15 and 16 show the evolution of the density as a function of AA mole fraction of the mixture, at a given temperature and pressure. As can be seen, increasing the content of AA in the mixture increases the density. The dependence of density on AA molar frac-

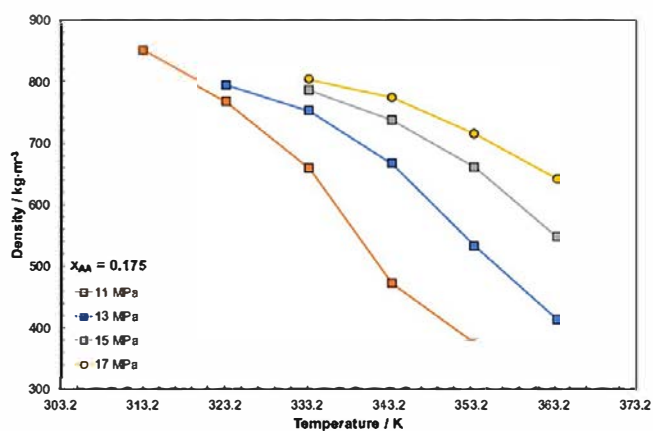


Fig. 11. Density vs temperature at constant overall composition ($x_{AA} = 0.175$) and constant pressure for the system AA + CO₂.

Experimental data (this work):

- (—■—) P = 11 MPa;
- (—■—) P = 13 MPa;
- (—■—) P = 15 MPa;
- (—●—) P = 17 MPa;

x_{AA} : AA mole fraction.

The straight lines were added to facilitate visualization.

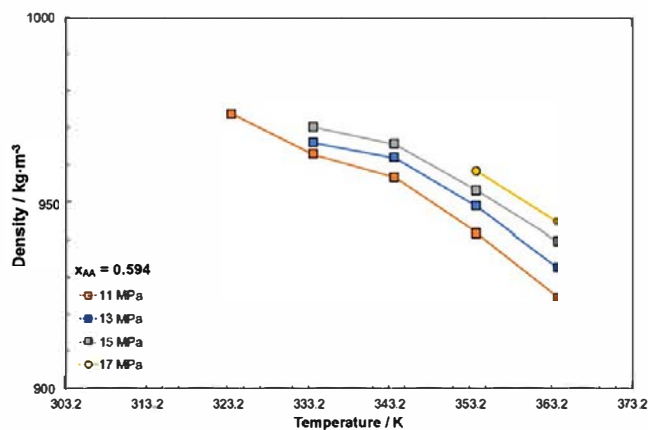


Fig. 14. Density vs temperature at constant overall composition ($x_{AA} = 0.594$) and constant pressure for the system AA + CO₂.

Experimental data (this work):

- (—■—) P = 11 MPa;
- (—■—) P = 13 MPa;
- (—■—) P = 15 MPa;
- (—●—) P = 17 MPa;

x_{AA} : AA mole fraction.

The straight lines were added to facilitate visualization.

tion is nonlinear. At intermediate composition, there is a steeper density increase with the addition of AA to the mixture. This effect can be attributed to the better packing of the liquid mixture and will be discussed in Section 3.3.

3.2. Phase boundaries

Phase behavior data can also be obtained from continuous pressure vs time recordings. As mentioned before, the abrupt slope change in pressure vs density curves corresponds to the onset of a new vapor phase when moving the piston backward and increasing the volume of the system, or to the collapse of the vapor into the liquid phase when moving the piston forward and decreasing the volume of the system. The phase boundaries obtained in this work

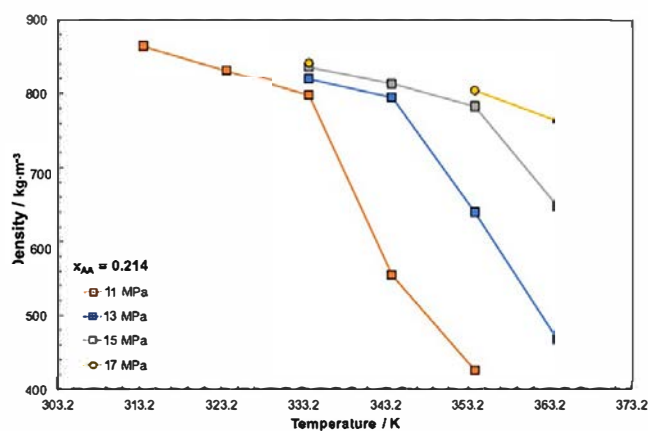


Fig. 12. Density vs temperature at constant overall composition ($x_{AA} = 0.214$) and constant pressure for the system AA + CO₂.

Experimental data (this work):

- (—■—) P = 11 MPa;
- (—■—) P = 13 MPa;
- (—■—) P = 15 MPa;
- (—●—) P = 17 MPa;

x_{AA} : AA mole fraction.

The straight lines were added to facilitate visualization.

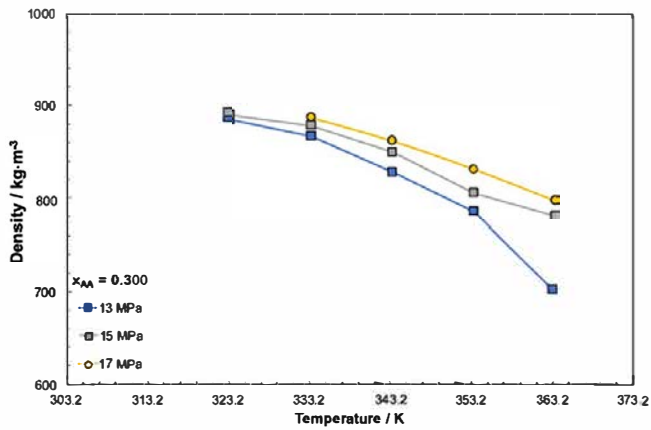


Fig. 13. Density vs temperature at constant overall composition ($x_{AA} = 0.300$) and constant pressure for the system AA + CO₂.

Experimental data (this work):

- (—■—) P = 13 MPa;
- (—■—) P = 15 MPa;
- (—●—) P = 17 MPa;

x_{AA} : AA mole fraction.

The straight lines were added to facilitate visualization.

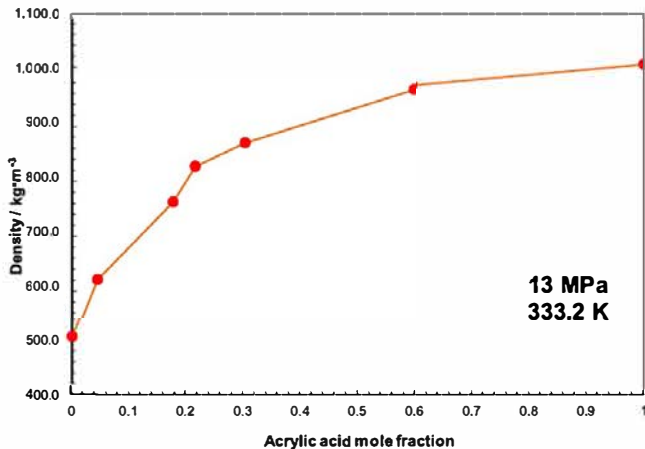


Fig. 15. Mass density vs composition (x_{AA}) at constant temperature (333.2 K) and constant pressure (13 MPa) for the system AA + CO₂.

x_{AA} : AA mole fraction.

The straight lines were added to facilitate visualization.

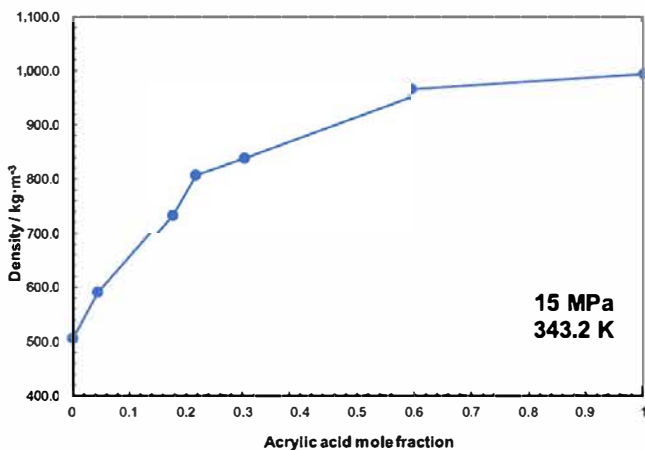


Fig. 16. Mass density vs composition (x_{AA}) at constant temperature (343.2 K) and constant pressure (15 MPa) for the system AA + CO₂.

x_{AA} : AA mole fraction.

The straight lines were added to facilitate visualization.

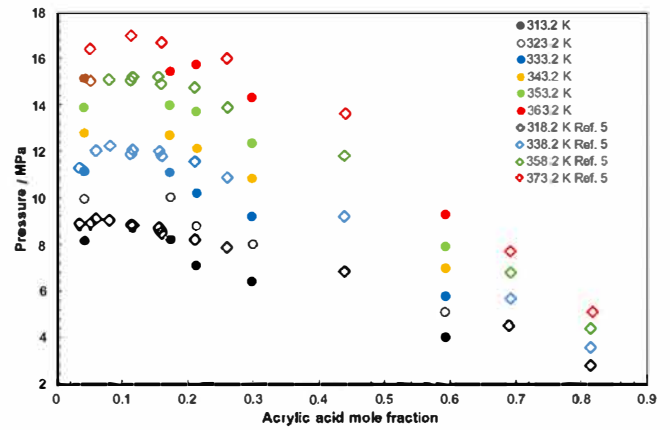


Fig. 17. Pressure vs composition (x_{AA}) at constant temperature for the system AA + CO₂.

Experimental data (this work):

- (●) T=313.2 K;
- (○) T=323.2 K;
- (●) T=333.2 K;
- (●) T=343.2 K;
- (●) T=353.2 K;
- (●) T=363.2 K;
- (◇) T=318.2 K (Ref. [5]);
- (◇) T=338.2 K (Ref. [5]);
- (◇) T=358.2 K (Ref. [5]);
- (◇) T=373.2 K (Ref. [5]);

x_{AA} : AA mole fraction.

are shown in Fig. 17. Four more data series were added to Fig. 17 to compare the data obtained in this work with the values reported by Byun et al. [5]. There is good agreement between the present values and the literature data. Table 1 shows the experimental phase boundaries obtained in this work, including the global composition of the mixture, the phase boundary pressure and the saturation density of the mixture. An additional line was added to Table 1 to show the saturation pressure and density of pure AA at given temperature. These values were calculated using correlations from the DIPPR database [23]. In all cases, as expected, the saturation densities of the mixtures are lower than the saturation density of pure AA.

The phase boundaries obtained were fitted using RKPR EoS with two adjustable parameters: k_{12} for the attractive parameter a and l_{12} for the co-volume of the mixture b . The pure compound parameters used in RKPR EoS are presented in Table 2, and the binary interaction parameters fitted for the phase boundaries of the binary system are presented in Table 3. Fig. 18 shows the results of the model fitting compared with the data obtained in this work. As it can be seen, there is a good representation of the phase boundaries, but, generally, at low AA content of the mixture, the EoS overpredicts the pressure of appearance of the new phase, and at higher AA composition, the EoS underpredicts the phase boundaries. Although the differences can be as high as 2 MPa in some cases (363.15 K and $x_{AA} = 0.594$), it is important to note that RKPR, as a simple cubic EoS model, can represent the main trends of the phase behavior of 'carboxylic acid + CO₂' binary mixture in the experimental window studied in this work. To avoid showing a single crowded Figure, the phase boundary data from Byun et al. [5] is shown in Fig. 19 using the same parameters as in Fig. 18 for the data obtained in this work. Again, at low AA concentration, the EoS overpredicts the phase boundaries (and the critical pressure of the mixture) and for high AA content mixtures, the EoS underpredicts the boundary pressures. The percentual average relative deviation

Table 1
Phase boundaries and saturation densities for CO₂ + AA (this work). Grey lines: pure AA saturation data extracted from DIPPR [23]. The percentual average relative deviation (ARD) is shown at the bottom of each isotherm.

Temperature [K]	AA mole fraction	Pressure [MPa]	Saturation density [kg/m ³]	Transition type*
313.15	0.044 ± 0.001	8.14	613 ± 10	DP
	0.175 ± 0.001	8.31	805 ± 13	BP
	0.214 ± 0.002	7.12	826 ± 16	BP
	0.300 ± 0.002	6.45	837 ± 9	BP
	0.594 ± 0.004	4.00	959 ± 10	BP
Ref. [23]	1.000	0.014	1028	
ARD (%)	6.24			
323.15	0.044 ± 0.001	9.91	497 ± 8	DP
	0.175 ± 0.001	10.00	729 ± 12	BP
	0.214 ± 0.002	8.87	803 ± 15	BP
	0.300 ± 0.002	8.04	849 ± 9	BP
	0.594 ± 0.004	5.10	952 ± 10	BP
Ref. [23]	1.000	0.0024	1017	
ARD (%)	8.82			
333.15	0.044 ± 0.001	11.12	485 ± 8	DP
	0.175 ± 0.001	11.06	678 ± 11	BP
	0.214 ± 0.002	10.19	784 ± 15	BP
	0.300 ± 0.002	9.18	840 ± 9	BP
	0.594 ± 0.004	5.77	938 ± 10	BP
Ref. [23]	1.000	0.0041	1005	
ARD (%)	6.74			
343.15	0.044 ± 0.001	12.81	454 ± 8	DP
	0.175 ± 0.001	12.68	660 ± 11	BP
	0.214 ± 0.002	12.14	781 ± 15	BP
	0.300 ± 0.002	10.84	792 ± 8	BP
	0.594 ± 0.004	6.99	937 ± 10	BP
Ref. [23]	1.000	0.0067	994	
ARD (%)	7.76			
353.15	0.044 ± 0.001	13.90	427 ± 7	DP
	0.175 ± 0.001	14.02	626 ± 10	BP
	0.214 ± 0.002	13.68	748 ± 14	BP
	0.300 ± 0.002	12.34	776 ± 8	BP
	0.594 ± 0.004	7.91	926 ± 10	BP
Ref. [23]	1.000	0.0105	982	
ARD (%)	7.02			
363.15	0.044 ± 0.001	15.16	397 ± 7	DP
	0.175 ± 0.001	15.45	587 ± 10	BP
	0.214 ± 0.002	15.75	743 ± 14	BP
	0.300 ± 0.002	14.30	778 ± 8	BP
	0.594 ± 0.004	9.260	909 ± 9	BP
Ref. [23]	1.000	0.0161	970	
ARD (%)	8.31			

u(T) = ±0.1 K. u(p) = ±0.13 MPa. u is the standard uncertainty in the measurement.

* BP: Bubble Point; DP: Dew Point.

Table 2
Pure compound parameters for the RKPR EOS used in this work.

	Carbon dioxide	Acrylic acid
<i>Acentric factor</i>	0.2236	0.5383
<i>a_c</i> (MPa·m ⁶ /mol ²)	0.38751 × 10 ⁻⁷	2.20618 × 10 ⁻⁶
<i>b</i> (m ³ /mol)	2.76 × 10 ⁻⁵	6.52 × 10 ⁻⁵
<i>δ</i> ₁	1.9722	3.3181

Table 3
RKPR EoS binary interaction parameters granted by the minimization of relative errors of bubble pressure.

	k _{ij}	l _{ij}
CO ₂ +AA	-0.06	-0.1

(%ARD) between experimental and predicted value is given at the end of each isotherm in Table 1. Although the prediction of the liquid densities obtained with the EoS was not quantitatively accurate, the general trends were well represented by the model. In general, the predicted liquid densities of the mixtures were always lower than the experimental values, mostly at high pressure. The model deviations increase with increasing carbon dioxide content of the mixture.

3.3. Excess volume

The excess volumes for the mixtures, representing the difference between real and ideal molar volume of the mixture, were determined from Eq. (2), where ρ_m is the density of the mixture and x_i , M_i , and ρ_i are the mole fraction, the molar mass, and the density of the component i , respectively:

$$V^E = \frac{x_{CO_2}M_{CO_2} + x_{AA}M_{AA}}{\rho_m} - \frac{x_{CO_2}M_{CO_2}}{\rho_{CO_2}} - \frac{x_{AA}M_{AA}}{\rho_{AA}} \quad (2)$$

In this relationship, densities are expressed on mass basis, whereas the resulting excess volumes are dimensionally on molar basis. Using the density data (in kg/m³) for the pure compounds and for the mixtures, and the molar mass values for CO₂ (0.04401 kg/mol) and AA (0.07206 kg/mol), the excess volumes (m³/mol of mixture) were evaluated as a function of the mole fraction of AA in the saturated liquid mixtures at different temperatures (333.15 and 343.15 K) at a given pressure of 15 MPa. The density of AA was considered as the saturated liquid density at 333.15 and 343.15 K, given that no experimental data of compressed liquid density was found in the literature. The results are shown in Fig. 20. The excess volumes are negative in the whole composition range. The minimum of the excess volume seems to be around $x_{AA} \cong 0.25$, a composition similar to those used for radical polymerization of

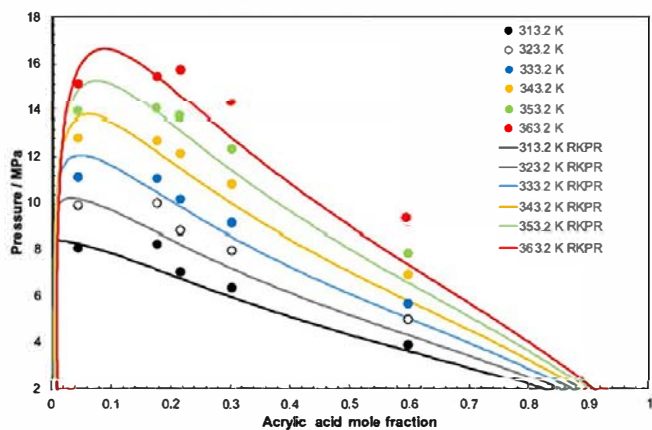


Fig. 18. Pressure vs composition (x_{AA}) at constant temperature for the system AA + CO₂.

Experimental data (this work):

- (●) T=313.2 K;
- (○) T=323.2 K;
- (●) T=333.2 K;
- (●) T=343.2 K;
- (●) T=353.2 K;
- (●) T=363.2 K;

Computed isotherms (Model: RKPR, $k_{CO_2,AA} = -0.06$, $l_{CO_2,AA} = -0.1$):

- (—) T = 313.2 K;
- (—) T = 323.2 K;
- (—) T = 333.2 K;
- (—) T = 343.2 K;
- (—) T = 343.2 K;
- (—) T = 363.2 K;

x_{AA} : AA mole fraction.

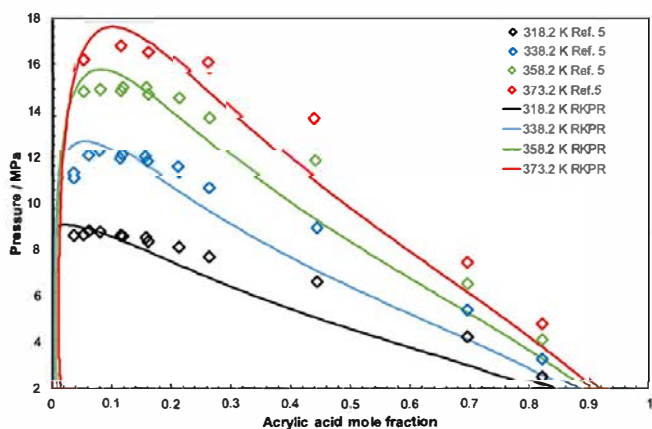


Fig. 19. Pressure vs composition (x_{AA}) at constant temperature for the system AA + CO₂.

Experimental data:

- (◇) T=318.2 K (Ref [5]);
- (◇) T=338.2 K (Ref [5]);
- (◇) T=358.2 K (Ref [5]);
- (◇) T=373.2 K (Ref [5]);

Computed isotherms (Model: RKPR, $k_{CO_2,AA} = -0.06$, $l_{CO_2,AA} = -0.1$):

- (—) T = 318.2 K;
- (—) T = 338.2 K;
- (—) T = 358.2 K;
- (—) T = 373.2 K.

x_{AA} : AA mole fraction.

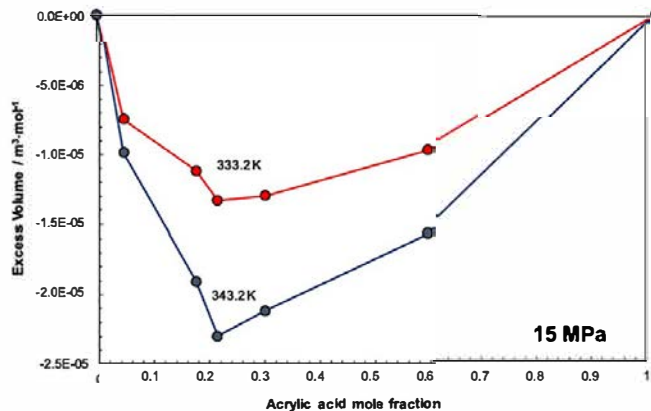


Fig. 20. Excess volume vs composition (x_{AA}) at constant temperature and constant pressure (15 MPa) for the system AA + CO₂.

Experimental data (this work):

- (—●—) T=333.2 K;
- (—●—) T=343.2 K.

x_{AA} : AA mole fraction.

The straight lines were added to facilitate visualization.

AA in carbon dioxide [2,7,11]. This composition appears to represent the mixture composition with the highest degree of packing. As introduced in Section 3.1 (Figs. 15 and 16) there is a packing effect of the mixture at intermediate compositions. The negative values of excess volume in mixtures are indicative of better packing, often arising in asymmetric systems that involve molecules of different sizes [24]. In the literature, the concept of “packing” in liquid mixtures was described for non-polar hydrocarbons of different sizes where small molecules fill the voids between larger molecules in analogy to dynamics observed in packing of solid particles. This approach shows an analogy between the porosity of a particle mixture at different states (i.e. the porosity depends on the state, e.g. packed or fluidized) and different temperatures for molecular mixtures (i.e. the ‘porosity’ depends on the temperature). Although the concept was developed for non-polar hydrocarbons, the idea can be extended to our mixture. Ease of rotation and accessibility of different conformational states for the biggest molecule of the mixture, i.e. AA, will be more difficult when temperature is lowered at a given pressure, unfavorably affecting the packing density and leading to less negative excess volumes. There are several references in the literature showing a negative excess volume in the whole compositional range for CO₂-containing mixtures at high pressure. Bessières et al. [25] measured excess volumes for ‘n-decane + CO₂’ mixtures, Kiran et al. [26] measured excess volumes for ‘acetone + CO₂’ mixtures and Smith Jr. et al. [27] measured excess volumes for ‘methanol + CO₂’ mixtures. The latter being the closely related system compared with ‘CO₂ + AA’ mixtures, given that methanol and AA are both polar compounds. The reported values by Smith Jr. et al. [27] are as low as $-20 \times 10^{-6} \text{ m}^3/\text{mol}$ at $x_{Methanol} \approx 0.25$, at 323.2 K and 11 MPa, while in the ‘CO₂ + AA’ data reported in this work, the excess volume is $-23 \times 10^{-6} \text{ m}^3/\text{mol}$ at $x_{AA} \approx 0.25$, at 343.2 K and 15 MPa.

Fig. 21 shows the molar volume of the mixture as a function of the AA molar fraction at 15 MPa for two different temperatures: 333.2 and 343.2 K. The negative deviation compared to the ideal solution is very clear. The ratio between the absolute value of the excess volume and the molar volume of the mixture at the same composition can be as high as 30 %. This represents a significant shrinkage of the mixture compared to an ideal solution.

This result could be important in radical batch supercritical polymerizations using CO₂ as the solvent, given that, as the reaction proceeds, the AA is consumed to form oligomers first and finally the

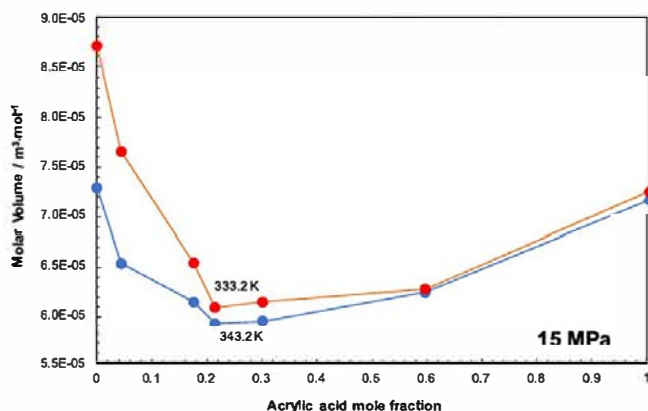


Fig. 21. Molar volume vs composition (x_{AA}) at constant temperature and constant pressure (15 MPa) for the system AA + CO₂.
fx18

polymer. Therefore, the composition of the CO₂ + AA binary mixture evolves inside the reactor. The pressure in a batch reactor should decrease or increase depending on the initial reactive composition, as long as the reaction progresses. If the initial composition is near $x_{AA} \approx 0.25$ [2,7,11], the pressure in a batch polymerization reactor can only increase.

4. Conclusions

Pseudo-continuous pressure vs density measurements were carried out for CO₂ + AA binary mixtures in the range of 313.15–363.15 K and up to 20 MPa. The data show that the density increases with the AA content of the mixture at a given temperature. Also, at a given composition, the density of the mixture increases with increasing pressure. As expected, for a given pressure, increasing temperature decreases the density of the mixture. This effect is less clear for mixtures with high AA content. Phase boundaries were obtained from the pressure vs density scans as the break point of a given isotherm. They show good agreement with previous data from literature. Modeling of the phase boundary data was made using RKPR EoS with two adjustable parameters: k_{12} and l_{12} . In general, there is a good representation of the phase boundaries. At low AA content of the mixture, the EoS overpredicts the pressure of appearance of the new phase and the critical point. At x_{AA} higher than 0.2, the model underpredicts the bubble pressures compared with the experimental measurements. The %ARD are less than 8.5 % for all isotherms measured in this work.

Excess volumes are highly negative in the whole composition range indicating better packing of the mixtures compared to the pure compounds. The largest negative values are observed at 0.25 AA mole fraction, a composition closely related to the initial reactive mixture for supercritical polymerization of AA. At a given pressure, higher temperatures lead to higher negative excess volumes. This result could have an impact on the pressure during batch polymerization in supercritical conditions.

Declaration of Competing Interest

None.

Acknowledgements

SEPPIC is gratefully acknowledged for financial support of this work. We also wish to thank to Consejo Nacional de Investigaciones Científicas y Técnicas de la República Argentina (CONICET) and Universidad Nacional de Córdoba (UNC).

Appendix A. Supplementary data

Supplementary material related to this article can be found, in the online version, at doi:<https://doi.org/10.1016/j.supflu.2020.104787>.

References

- [1] E. Alper, O. Yuskel Orhan, CO₂ Utilization: developments in conversion processes, *Petroleum*. 3 (2017) 109–126, <http://dx.doi.org/10.1016/j.petlm.2016.11.003>.
- [2] T.J. Romack, E.E. Maury, J.M. DeSimone, Precipitation polymerization of acrylic acid in supercritical carbon dioxide, *Macromolecules* 28 (1995) 912–915, <http://dx.doi.org/10.1021/ma00108a017>.
- [3] M. Mukhopadhyay, Extraction and processing with supercritical fluids, *J. Chem. Technol. Biotechnol.* 84 (2009) 6–12, <http://dx.doi.org/10.1002/jctb.2072>.
- [4] R.B. Gupta, J.-J. Shim, *Solubility in Supercritical Carbon Dioxide*, CRC Press, 2007.
- [5] H.-S. Byun, B.M. Hasch, M.A. Mchugh, Phase behavior and modeling of the systems CO₂-acetonitrile and CO₂-acrylic acid, *Fluid Phase Equilib.* 115 (1996) 179–192, [http://dx.doi.org/10.1016/0378-3812\(95\)02830-7](http://dx.doi.org/10.1016/0378-3812(95)02830-7).
- [6] C. Boyère, C. Jérôme, A. Debuigne, Input of supercritical carbon dioxide to polymer synthesis: an overview, *Eur. Polym. J.* 61 (2014) 45–63, <http://dx.doi.org/10.1016/j.eurpolymj.2014.07.019>.
- [7] T. Liu, J.M. DeSimone, G.W. Roberts, Continuous precipitation polymerization of acrylic acid in supercritical carbon dioxide: the polymerization rate and the polymer molecular weight, *J. Polym. Sci. Part A: Polym. Chem.* 43 (2005) 2546–2555, <http://dx.doi.org/10.1002/pola.20728>.
- [8] J. Chen, X. Liu, Z. Liu, D. Hu, C. Zhang, D. Xue, J. Xiao, Z. Liu, Intermolecular-interaction-dominated solvation behaviors of liquid monomers and polymers in gaseous and supercritical carbon dioxide, *Macromolecules* 45 (2012) 4907–4919, <http://dx.doi.org/10.1021/ma300556z>.
- [9] R. Arshady, Suspension, emulsion, and dispersion polymerization: a methodological survey, *Colloid Polym. Sci.* 270 (1992) 717–732, <http://dx.doi.org/10.1007/bf00776142>.
- [10] J.G. Tsavalas, Emulsion copolymerization (also leading to core-shell structures), in: S. Kobayashi, K. Müllen (Eds.), *Encyclopedia of Polymeric Nanomaterials*, Springer, Berlin, Heidelberg, 2015.
- [11] J.-N. Ollagnier, T. Tassaing, S. Harrison, M. Destarac, Application of online infrared spectroscopy to study the kinetics of precipitation polymerization of acrylic acid in supercritical carbon dioxide, *React. Chem. Eng.* 1 (2016) 372–378, <http://dx.doi.org/10.1039/C6RE00022C>.
- [12] G. Herth, G. Schornick, F.L. Buchholz, *Polyacrylamides and Poly(Acrylic Acids)*, *Ullmann's Encyclopedia of Industrial Chemistry*, 2015, pp. 1–16.
- [13] Q. Xu, B. Han, H. Yan, Precipitation polymerization of acrylic acid in compressed carbon dioxide – cosolvent systems, *J. Appl. Polym. Sci.* 88 (2003) 1876–1880, <http://dx.doi.org/10.1002/app.11908>.
- [14] T. Liu, J.M. DeSimone, G.W. Roberts, Kinetics of the precipitation polymerization of acrylic acid in supercritical carbon dioxide: the locus of polymerization, *Chem. Eng. Sci.* 61 (2006) 3129–3139, <http://dx.doi.org/10.1016/j.ces.2005.11.052>.
- [15] J.M. Milanesio, J.C. Hassler, E. Kiran, Volumetric properties of propane, n-octane, and their binary mixtures at high pressures, *Ind. Eng. Chem. Res.* 52 (2013) 6592–6609, <http://dx.doi.org/10.1021/ie4007084>.
- [16] N. Falco, E. Kiran, Volumetric properties of ethyl acetate + carbon dioxide binary fluid mixtures at high pressures, *J. Supercrit. Fluids* 61 (2012) 9–24, <http://dx.doi.org/10.1016/j.supflu.2011.09.016>.
- [17] H.E. Grandelli, E. Kiran, High pressure density, Miscibility and compressibility of poly(lactide-co-glycolide) solutions in acetone and acetone + CO₂ binary fluid mixtures, *J. Supercrit. Fluids* 75 (2013) 159–171, <http://dx.doi.org/10.1016/j.supflu.2012.12.034>.
- [18] M. Cismondi, J. Mollerup, Development and application of a three-parameter RK – PR equation of state, *Fluid Phase Equilib.* 232 (2005) 74–89, <http://dx.doi.org/10.1016/j.fluid.2005.03.020>.
- [19] S. Sima, J.M. Milanesio, J.I. Ramello, M. Cismondi, C. Secuianu, V. Feroiu, D. Geana, The effect of the naphthenic ring on the VLE of (Carbon dioxide + alkane) mixtures, *J. Chem. Thermodyn.* 93 (2016) 374–385, <http://dx.doi.org/10.1016/j.jct.2015.07.018>.
- [20] M. Cismondi, S.B. Rodriguez-Reartes, J.M. Milanesio, M.S. Zabaloy, Phase equilibria of CO₂ + n-Alkane binary systems in wide ranges of conditions: development of predictive correlations based on cubic mixing rules, *Ind. Eng. Chem. Res.* 51 (2012) 6232–6250, <http://dx.doi.org/10.1021/ie2018806>.
- [21] M. Cismondi, J.M. Mollerup, M.S. Zabaloy, Equation of state modeling of the phase equilibria of asymmetric CO₂+n-alkane binary systems using mixing rules cubic with respect to mole fraction, *J. Supercrit. Fluids* 55 (2010) 671–681, <http://dx.doi.org/10.1016/j.supflu.2010.10.007>.
- [22] E.W. Lemmon, M.O. McLinden, D.G. Friend, in: P.J. Linstrom, W.G. Mallard (Eds.), "Thermophysical Properties of Fluid Systems" en NIST Chemistry WebBook, NIST Standard Reference Database Number 69, National Institute of Standards and Technology, Gaithersburg MD, 2020, p. 20899, <http://dx.doi.org/10.18434/T4D303> (September 17th, 2019).

- [23] DIPPR-801. Evaluated Process Design Data, Public Release. American Institute of Chemical Engineers, Design Institute for Physical Property Data, BYU-DIPPR. Provo, Thermophysical Properties Laboratory, Utah, 2003.
- [24] H.J. Finkers, J.C. Bosma, A.A. Broekhuis, A novel approach to predict the excess volume of hydrocarbon mixtures, *Chem. Eng. Sci.* 66 (2011) 2889–2897, <http://dx.doi.org/10.1016/j.ces.2011.02.007>.
- [25] D. Bessières, H. Saint-Guirons, J.-L. Daridon, Volumetric behavior of decane + carbon dioxide at high pressures. measurement and calculation, *J. Chem. Eng. Data* 46 (2001) 1136–1139, <http://dx.doi.org/10.1021/je010016k>.
- [26] E. Kiran, H. Pöhler, Y. Xiong, Volumetric properties of pentane + carbon dioxide at high pressures, *J. Chem. Eng. Data* 41 (1996) 158–165, <http://dx.doi.org/10.1021/je9501503>.
- [27] R.L. Smith Jr., C. Saito, S. Suzuki, S.-B. Lee, H. Inomata, K. Arai, Temperature dependence of dielectric spectra of carbon dioxide and methanol mixtures at high-pressures, *Fluid Phase Equilib.* 194–197 (2002) 869–877, [http://dx.doi.org/10.1016/S0378-3812\(01\)00714-2](http://dx.doi.org/10.1016/S0378-3812(01)00714-2).